

*Original article*

## Spots and turbulent domains in a model of transitional plane Couette flow

Paul Manneville

Laboratoire d'Hydrodynamique, UMR CNRS 7646, Ecole polytechnique, Palaiseau, France  
(e-mail: paul.manneville@ladhyx.polytechnique.fr)

Received October 15, 2003 / Accepted May 25, 2004  
Published online October 7, 2004 – © Springer-Verlag 2004  
Communicated by H.J.S. Fernando

**Abstract.** A review of the *globally subcritical* transition to turbulence in shear flows is presented, with an emphasis on the cases of plane and circular Couette flows (pCf and cCf, respectively). A Swift–Hohenberg-like model is next proposed to interpret the behavior of plane Couette flow in the vicinity of its global stability threshold. We present results of numerical simulations supporting this proposal and helping us to raise “good” questions about the growth and decay of intermittent turbulent domains in this precise context, and more generally about the coexistence of laminar flow and turbulence in other spatio-temporally intermittent flows.

**Key words:** Couette flow, transition to turbulence, Galerkin modeling

**PACS:** 47.27.-i, 47.54.-r, 05.45.-a

### 1 General setting

The transition to turbulence is fairly well understood as a cascade toward more and more flow complexity when there exists a linear instability mechanism, then gentle saturation of the unstable mode, a subsequent secondary instability, and so on, i.e., a *globally supercritical* scenario. Things are much more difficult to grasp when the linear instability threshold is difficult to reach before the system has jumped to a state which, in some sense, is far from the base flow, a situation that can be called *globally subcritical* (see Manneville and Dauchot [23] for an introduction to the terminology used here).

The best known prototype of systems experiencing a globally supercritical transition to turbulence is plain Rayleigh–Bénard convection. Other examples are the Taylor–Couette centrifugal instability when the inner cylinder rotates faster and in the same direction as the outer cylinder, or else open flows such as mixing layers, with base velocity profiles displaying inflection points of the Rayleigh–Fjørtoft-unstable type and experiencing a Kelvin–Helmholtz-like instability, see e.g., the introductory book by Drazin [11].

By contrast and generally speaking, the globally subcritical scenario takes place in open flows when the base profile is mechanically stable (no inflection point). The linear instability threshold may then be associated to Tollmien–Schlichting waves generation by subtle feedbacks involving viscous effects in a crucial way, see e.g., Huerre and Rossi [18]. For example, the plane Poiseuille flow is linearly unstable at Reynolds number  $R_c = 5772$  (Orszag [27]), the instability is (locally) subcritical and the bifurcated branch turns back

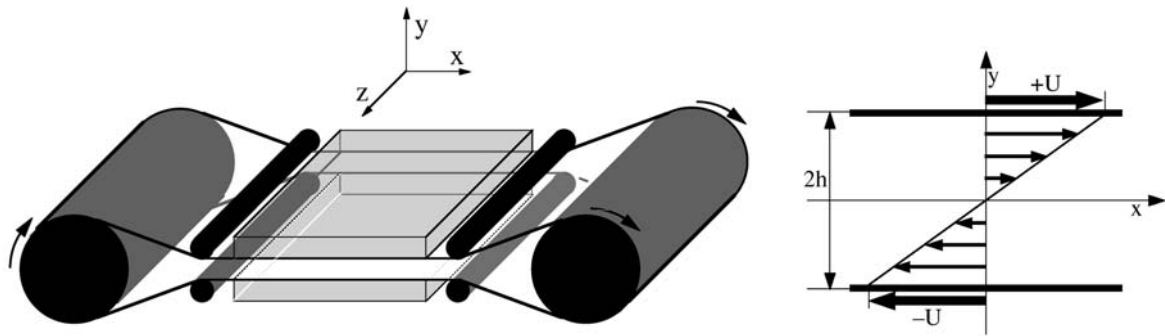


Fig. 1. Left: Experimental set-up. Right: laminar regime with a linear velocity profile

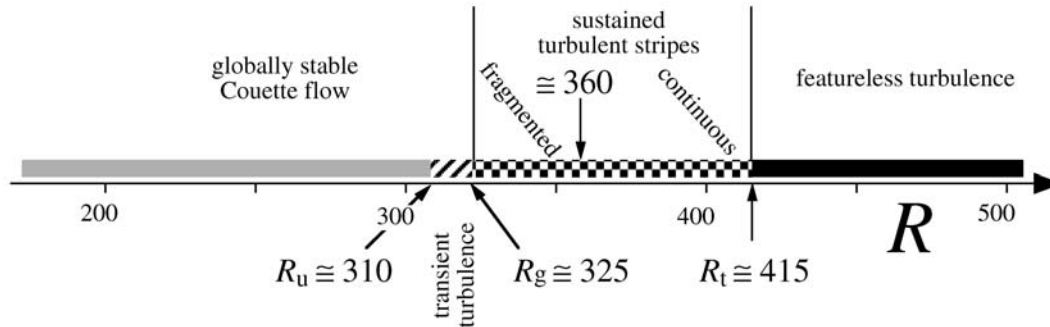


Fig. 2. Bifurcation diagram of plane Couette flow

at  $R_{nl} \simeq 2\,900$  through a saddle–node bifurcation (Herbert [17]), but the flow can carry sustained turbulent spots for  $R$  as low as about 1000 (Carlson et al. [5]).

The circular Couette flow (cCf) is another interesting case since, when the two cylinders rotate sufficiently fast in opposite directions, it is centrifugally unstable only close to the inner cylinder and the corresponding layer can become irrelevant because the flow has jumped to the celebrated turbulent spiral regime described by Coles [8]. Keeping the trace of curvature effects, inertial forces of centrifugal origin, and other mechanisms responsible for, e.g., the sustainment of that regime, the cCf's bifurcation diagram is complicated. Two different radius ratios (curvatures) were chosen by Andereck et al. [1] and Prigent et al. [30],  $\eta = 0.883$  and  $0.983$  respectively. A simpler configuration, presumably a good candidate for an isolated study of these mechanisms, is plane Couette flow (pCf) obtained by shearing a fluid between two walls sliding parallel to each other in opposite direction. The resulting linear velocity profile was shown to be linearly stable for all Reynolds numbers ( $R_c = \infty$ ) by Romanov [33] though turbulence can be observed above some global stability threshold  $R_g$  that has been for long the subject of numerous experimental or numerical studies. For a review with references, consult Manneville and Dauchot [23].

Just to fix the ideas let us briefly summarize the experimental results recently obtained in Saclay and described elsewhere in detail. The set-up is sketched in Fig. 1 (left), showing a fluid sheared by a plastic loop guided and driven by sets of rolls. The Reynolds number is defined as  $R = Uh/\nu$  where  $\nu$  is the kinematic viscosity of the fluid (water),  $U$  is the linear speed of the loop and  $2h$  is the gap between the two facing parts of the band, as illustrated in Fig. 1 (right).

The bifurcation diagram inferred from experiments by O. Dauchot and his collaborators, is displayed in Fig. 2. Below  $R_u \simeq 310$ , all perturbations decay and the flow rapidly return to the base state. Between  $R_u$  and  $R_g \simeq 325$ , instantaneous perturbations introduced in the flow generate turbulent spots but these spots have a finite lifetime. This lifetime diverges as  $R_g$  is approached from below and beyond this value, most of them do not decay (Bottin et al. [3]). When  $R$  is further increased and the aspect ratio is large enough, spots arrange themselves to form oblique stripes, irregular and fragmented below  $R \sim 360$ , regular and continuous above. The modulation of turbulent intensity associated to the stripes then progressively decreases and a regime of featureless turbulence prevails beyond  $R_t = 415$  as shown by Prigent et

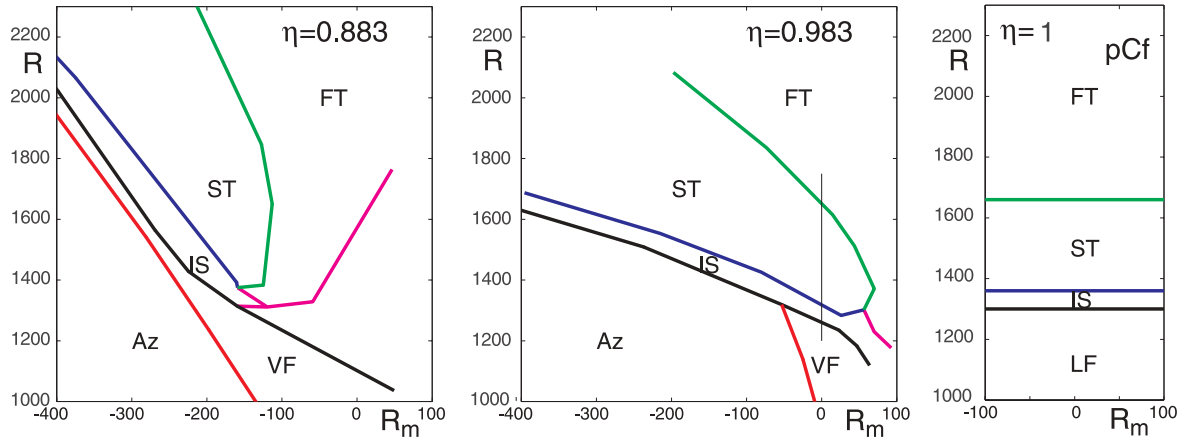


**Fig. 3.** Bifurcation diagram for cCf after [1], [30] using  $R$  and  $R$  instead of  $R_{i,o}$  and for pCf using  $\tilde{R} = 4R$

al. [30]. This sequence is strongly reminiscent of the corresponding one in the Taylor–Couette apparatus between counter-rotating cylinders, and even at the quantitative level provided that the Reynolds number is defined not as usual but based on the shear rate and the viscous time over the full gap, which yields  $\tilde{R} = (U/h)/(v/(2h))^2 = 4R$ . This is demonstrated in Fig. 3 which displays the cCf bifurcations diagrams obtained by Andereck et al. [1], and Prigent et al. [30], and plane Couette flow quoted in Fig. 2. (The occurrence of wavy Taylor vortices in the limit  $\eta \rightarrow 1$  was studied by Faisst and Eckhardt [14] in connection with pCf nontrivial nonlinear structures called the Nagata–Busse–Clever states, independently discovered by Nagata [26] and Clever and Busse [7].) Diagrams for cCf are redrawn from original data by changing from the usual Reynolds numbers in terms of cylinder speeds  $R_{i,o} = \omega_{i,o} r_{i,o} (r_o - r_i)/\nu$ , with  $\omega_i > 0$  by convention and thus  $R_o < 0$  when cylinders are counter-rotating, to quantities defined using the average shear rate  $R = \frac{2}{1+\eta}(R_i - \eta R_o)$ , and the average angular speed  $R_m = \frac{1+\eta}{4\eta}(R_1 + \eta R_2)$  where  $\eta = r_i/r_o$ . In the case of pCf, we use for  $R$  the Reynolds number based on the shear, previously called  $\tilde{R}$ . There is of course no average rotation for pCf but its role is played by streamwise translation which has no effect on thresholds owing to Galilean invariance. In these diagrams, ‘Az’ means azimuthal Couette flow, ‘VF’ is Taylor vortex flow (possibly wavy Taylor vortex flow, since in the present context there is no need to make the difference), ‘IS’ is for Intermittent Spirals (cCf) or Stripes (pCf), ‘ST’ is Spiral (cCf) or Stripe (pCf) Turbulence, and ‘FT’ stands for Featureless Turbulence. The effect of curvature is clear from the comparison of the two left panels: when  $\eta$  increases, the domain of Taylor vortices is shifted to the right and the Rayleigh instability mechanism based on rotation effects is less and less relevant. The vertical piece of line in the diagram for  $\eta = 0.983$  corresponds to zero average rotation, and thus to a scenario where phenomena appear at rest when seen from the laboratory frame. In the diagram for pCf ( $\eta = 1$ ) ‘LF’ corresponds to uniform laminar flow and thus to ‘Az’ when  $\eta < 1$ . For  $\eta = 0.983$  the ‘VF’ regime is not yet evacuated for  $R_m = 0$  but nearly so and thresholds for the nucleation of intermittent turbulent domains, their conversion into continuous spirals or stripes and the final transition to the FT regime are strikingly similar. These diagrams were shown for the first time at the San Diego DFD01 conference (Manneville et al. [25]). Interestingly enough the value of the threshold for global stability in terms of shear  $\simeq 1300$  for pCf is also of the same order of magnitude as the value below which spots are no longer sustained in the plane Poiseuille flow according to Carlson et al. [5]. A similar remark might be made for transitional boundary layers but this would demand to know more precisely the value of the Reynolds number at which the precursors of turbulent spots resulting from the break-down of secondary modes of Tollmien–Schlichting waves, called spikes, appear in the flow; the actual situation is furthermore obscured by the fact that the Reynolds number increases downstream in that case. Torsional Couette flow, the flow obtained by rotating two disks around an axis perpendicular to their plane and studied, e.g., by Cros and Le Gal [9] is still another example where spots appear in the system in precisely the same range of Reynolds numbers  $\sim 10^3$  when defined properly from the local shear rate and the viscous relaxation time.

Transitional plane Couette flow mainly poses two problems: (1) how spots get sustained at moderate  $R$ , and (2) how the turbulent modulation disappears to yield featureless turbulence at large  $R$  without apparent hysteresis.

Problem (2) has been quantitatively studied in the Taylor–Couette case, though no real explanation has been given. The transition is well accounted for in terms of standard pattern formation and Ginzburg–Landau formalism, provided that the classical picture is completed by a high level of additive noise presumably due to the turbulent background in the featureless regime (Prigent et al. [31]). A similar description is expected to hold for the plane Couette flow. This problem will not be addressed in the following.

Problem (1) has been approached in different ways besides laboratory experiments already mentioned, from conceptual arguments, in particular by Pomeau [28], to numerical simulations of primitive equations, see e.g., Lundbladh and Johansson [20] or Reddy et al. [32], modeling attempts, e.g., Waleffe [40] or Eckhardt and Mersmann [13], and to analytic studies, mainly through bounds on perturbation energy, especially by Chapman [6] who gives references to earlier work. See also the book by Schmid and Henningson [34], Chapter 9, for a more general viewpoint on mechanisms in similar flow configurations.

A detailed understanding of the globally subcritical transition to turbulence via turbulent spots relies both on a description of “microscopic” processes such as the generation of streamwise vortices, the amplification of streaks through transient energy growth, and the subsequent instability, discussed by many authors and in particular by Hamilton et al. [15]. On the other hand, a fully abstract point of view, with a more “macroscopic” flavor, was taken by Pomeau [28] who discussed the question of coexistence between laminar flow and turbulence as a nucleation problem in terms of first-order phase transitions. He elaborated on the correspondence between this context and that of standard subcritical bifurcations, but without giving any specific meaning to the “thermodynamic” potential so introduced and the corresponding “Maxwell plateau” for phase coexistence. He argued that when one of the competing states was “chaotic” the competition could be understood in terms of a stochastic contamination process in the same universality class as *directed percolation*, thus bridging two fields, hydrodynamics and statistical physics, in a spirit rather different from that implied in the Ruelle–Takens conjecture about the nature of turbulence bridging hydrodynamics to mathematics through the concept of chaos.

In Sect. 2 we present our “semi-microscopic” modeling approach to problem (1) attempting at a reconciliation of the microscopic and macroscopic viewpoints exposed above and next, in Sect. 3, some numerical simulations results obtained from the model on spots dynamics and turbulent domain growth or decay. Perspectives are presented in Sect. 4.

## 2 The model and some basic properties

Progress in the understanding of the so-called *bypass* transition that corresponds to our globally subcritical scenario is expected perhaps no longer from the detailed study of output of direct numerical simulations or analytical approaches but rather from modeling that provide heuristic explanations to be further tested in experiments either in the laboratory or in the computer. Most rational modeling approaches are developed through truncations of appropriate Galerkin expansions of the primitive equations. Rayleigh–Bénard convection can serve us as an example. The celebrated Lorenz model was obtained by expanding the unrealistic stress-free Boussinesq equations used initially by Rayleigh on a Fourier basis by retaining only one cross-variable mode and one in-plane Fourier mode, closing the system through a first-harmonic approximation, ending with a set of three quadratically-coupled differential equations (Lorenz [19]). Approximations made are acceptable only in the case of strong confinement effects turning the transition to turbulence as a *temporal chaos* problem. On the other hand, Swift and Hohenberg [37] derived a model in terms of a single partial differential equation for a semi-microscopic field featuring convection in extended geometry when confinement effects are weak. The starting point was the same but emphasis was placed on *patterns* with a trivial cross-variable dependence. In Manneville [21], this model was later extended to deal with secondary flows generated by the non-ideal features of the patterns (curvature, defects) and could be used to approach the problem of transition to turbulence in convection at low Prandtl numbers, especially *via* spiral turbulence. Our modeling approach basically follows the same line that goes from temporal to spatio-temporal chaos, from the Lorenz model to the extended Swift–Hohenberg model.

Modeling the plane Couette flow with strong in-plane periodicity constraints has been developed by Eckhardt and Mersmann [13] who derived a 19-dimensional differential dynamical system, cleverly closed but for modes with complicated spatial structure not obviously related to the streaks and streamwise vortices clearly apparent in the transition. Well in the spirit of temporal chaos theory, their model was used to study the transition between chaotic transients and sustained chaos corresponding to the global stability threshold. By contrast, Waleffe [39] injected the expected physical nature of the modes directly in the Galerkin decomposition, obtaining a much more transparent system of four differential equations, easier to study in detail. The variables in his model were clearly identified as a mean flow correction and lowest Fourier harmonics accounting for the streak and streamwise vortices. Unfortunately, in the range of parameters of interest for its actual application, the model has no chaotic attractor but only stable and unstable fixed points, and an unstable limit cycle. As shown in particular by Dauchot and Vioujard [10], close to the global stability threshold, the stable manifold of the unstable limit cycle gives much complexity to the structure of the attraction basins of the trivial base state and the competing nonlinear nontrivial state, which results in a statistical behavior of transient lifetimes mimicking those observed in actual pCf. At any rate, such definitely low-dimensional dynamical systems seem inappropriate to deal with the irreducible spatio-temporal features of problem (1), which we want to reintroduce in the spirit of Swift–Hohenberg modeling.

The model introduced in Manneville and Locher [24] and extending Waleffe’s approach to the case of pCf in extended geometry, derives straightforwardly from an application of the Galerkin method to the Navier–Stokes equations for an incompressible flow in the geometry of Fig. 1. In dimensionless form the primitive equations read:

$$\partial_t \mathbf{v} + \mathbf{v} \cdot \nabla \mathbf{v} = -\nabla p + R^{-1} \nabla^2 \mathbf{v} + \mathbf{F}, \quad (1)$$

$$\nabla \cdot \mathbf{v} = 0, \quad (2)$$

where  $R$  is the Reynolds number defined as usual by  $R = Uh/\nu$ ,  $h$  and  $h/U$  being the space and time units, respectively.

The physical no-slip boundary conditions are replaced by idealistic stress-free conditions at  $y = \pm 1$ , and this is precisely the reason why a force  $\mathbf{F}$  adjusted to drive the fluid must be added on the r.h.s. of Eq. (1). Following Waleffe [39] we assume a base flow profile in the form  $u_b = \sin(\beta y)$  with  $\beta = \pi/2$  and take  $\mathbf{F}(y) = F \sin(\beta y) \hat{\mathbf{x}}$  with  $F = \beta^2/R$ .

The problem is then written for the perturbation:

$$\{u', w', p'\} = \{U_0, W_0, P_0\} + \sum_{k \geq 1} \{U_{2k-1}, W_{2k-1}, P_{2k-1}\} \sin((2k-1)\beta y) \quad (3)$$

$$+ \{U_{2k}, W_{2k}, P_{2k}\} \cos(2k\beta y) \quad (4)$$

$$v' = \sum_{k \geq 1} V_{2k-1} \cos((2k-1)\beta y) + V_{2k} \sin(2k\beta y), \quad (5)$$

where all the expansion coefficients are functions of remaining space coordinates  $(x, z)$  and time  $t$ , in the spirit of the work by Swift and Hohenberg [37].

Ultimately the expansions are truncated beyond some index  $k$ , leaving us with a closed *2.5-dimensional* model appropriate to study weakly turbulent regimes mostly understood as spatio-temporal chaos. Here ‘2.5’ means ‘2’ for the  $(x, z)$  dependence and ‘.5’ for the  $y$  dependence, which is dealt with explicitly through a low resolution modal decomposition. This is in contrast with accurate but analytically opaque pseudo-spectral projections used in direct numerical simulations (as those of Schumacher and Eckhardt [36] for stress-free pCf) but the objective of our model is definitely not the same. What is searched is not numerical exactness, but the possibility to push the analysis as far as possible, even if we will not go in that direction in the present paper, but, on the contrary, just present numerical results supporting the idea that the model might bring a valuable contribution to the study of globally subcritical transitions to turbulence.

Whereas different harmonics in the cross-stream dependence are left uncoupled by the linear terms in Eq. (1), the advection nonlinearity introduce some coupling between these harmonics. Before showing how the model can be enlarged to include more modes, let us present its truncation at lowest significant order, to be used in the sequel, i.e., just involving harmonic zero  $\{U_0, W_0\}$ , and one  $\{U_1, W_1\} \sin(\beta y)$ ,  $V_1 \cos(\beta y)$ , and the corresponding pressure terms  $P_0$  and  $P_1 \sin(\beta y)$ .

First the continuity Eq. (2) obviously leads to two uncoupled equations:

$$\partial_x U_0 + \partial_z W_0 = 0, \quad (6)$$

$$\partial_x U_1 + \partial_z W_1 = \beta V_1. \quad (7)$$

This nice property is unfortunately broken by the advection term in Eq. (1) in two ways giving several kinds of terms. A first obvious series of terms arises from the nonlinear couplings of fluctuations between themselves, while other less obvious terms originate from the coupling of fluctuations to the base flow, which introduces the so-called non-normal terms. Inserting Eq. (3) in this equation, expanding the products, and isolating the terms that are independent of  $y$ , keeping only terms with indices '0' and '1', we get:

$$\partial_t U_0 + N_{U_0} = -\partial_x P_0 - \frac{1}{2} \partial_x U_1 - \frac{1}{2} \beta V_1 + R^{-1} \Delta_2 U_0, \quad (8)$$

$$\partial_t W_0 + N_{W_0} = -\partial_z P_0 - \frac{1}{2} \partial_x W_1 + R^{-1} \Delta_2 W_0, \quad (9)$$

with  $\Delta_2 \equiv \partial_{xx} + \partial_{zz}$ , the terms responsible for non-normality have been placed on the r.h.s. while the nonlinear advection terms on the l.h.s. read:

$$N_{U_0} = U_0 \partial_x U_0 + W_0 \partial_z U_0 + \frac{1}{2} (U_1 \partial_x U_1 + \beta V_1 U_1 + W_1 \partial_z U_1), \quad (10)$$

$$N_{W_0} = U_0 \partial_x W_0 + W_0 \partial_z W_0 + \frac{1}{2} (U_1 \partial_x W_1 + \beta V_1 W_1 + W_1 \partial_z W_1). \quad (11)$$

In the same way the equations for the terms in  $\sin(\beta y)$  read:

$$\partial_t U_1 + N_{U_1} = -\partial_x P_1 - \partial_x U_0 + R^{-1} (\Delta_2 - \beta^2) U_1, \quad (12)$$

$$N_{U_1} = U_0 \partial_x U_1 + W_0 \partial_z U_1 + U_1 \partial_x U_0 + W_1 \partial_z U_0, \quad (13)$$

$$\partial_t W_1 + N_{W_1} = -\partial_z P_1 - \partial_x W_0 + R^{-1} (\Delta_2 - \beta^2) W_1, \quad (14)$$

$$N_{W_1} = U_0 \partial_x W_1 + W_0 \partial_z W_1 + U_1 \partial_x W_0 + W_1 \partial_z W_0, \quad (15)$$

and that for the term in  $\cos(\beta y)$ :

$$\partial_t V_1 + N_{V_1} = -\beta P_1 + R^{-1} (\Delta_2 - \beta^2) V_1, \quad (16)$$

$$N_{V_1} = U_0 \partial_x V_1 + W_0 \partial_z V_1. \quad (17)$$

In all these equations, terms in factor of  $R^{-1}$  account for viscous dissipation.

The pressure field can be eliminated by introducing appropriate stream-functions and potentials. The flow component  $\{U_0, W_0\}$  is described by a stream-function  $\Psi_0$  such that:

$$U_0 = -\partial_z \Psi_0 \quad \text{and} \quad W_0 = \partial_x \Psi_0,$$

The rest of the flow,  $\{U_1, V_1, W_1\}$ , can be decomposed into two part, rotational and irrotational, requiring two fields for their description, a potential  $\Phi_1$  and a stream-function  $\Psi$ , which gives:

$$U_1 = \partial_x \Phi_1 - \partial_z \Psi_1 \quad \text{and} \quad W_1 = \partial_z \Phi_1 + \partial_x \Psi_1,$$

while  $V_1$  is derived from the continuity Eq. (7) that now reads:

$$\beta V_1 = \Delta_2 \Phi_1.$$

The final expression of the model is therefore a system of three partial differential equations for the three two-dimensional fields,  $\Psi_0, \Psi_1, \Phi_1$ .

Truncation at higher order implies straightforward but tedious computations. The generalization of Eq. (7) is easily obtained as

$$\partial_x U_k + k\beta(-1)^k V_k + \partial_z W_k = 0$$

further taken into account through the introduction of two new fields  $\Phi_k$  and  $\Psi_k$ , etc. Non-normal terms arise from the expansion of terms such as  $u_b \partial_x u'$ , which gives terms in  $\sin(\beta y) \sin((2k-1)\beta y) \partial_x U_{2k-1}$  and  $\sin(\beta y) \cos(2k\beta y) \partial_x U_{2k}$  that are further reduced to sums of cosines or sines using standard trigonometric relations. For example  $\sin(\beta y) \cos(2k\beta y) = \frac{1}{2}[\sin((2k+1)\beta y) + \sin((2k-1)\beta y)]$ , which implies the presence of a term  $\partial_x U_{2k}$  in equations for  $U_{2k-1}$  and  $U_{2k+1}$ . Nonlinear terms are even more complicated since the expansion of products, e.g.,  $u' \partial_x u'$  generate double sums of products involving sines or cosines of various multiples of  $\beta y$ . Only the terms in equations for  $U_0$  and  $W_0$  are easily guessed, e.g.,

$$N_{U_0} = U_0 \partial_x U_0 + W_0 \partial_z U_0 + \frac{1}{2} \sum_k U_k \partial_x U_k - k\beta(-1)^k V_k U_k + W_k \partial_z U_k,$$

but there is no real need to go beyond this sketchy presentation. The models obtained by truncation beyond  $k = 2$  are currently dealt with by M. Lagha at LadHyX.

The origin of each term in the model is easily identifiable and, in particular, the nonlinear terms clearly have the structure of advection terms and the non-normal terms work as expected (see e.g., when  $V_1 > 0$ , term  $-\beta V_1$  in Eq. (8) imply  $\partial_t U_0$ , i.e., tends to decrease  $U_0$  by bringing slow fluid from below, which here expresses the *lift-up* mechanism).

Some immediate properties of the model are worth mentioning. It can first be checked that these terms ( $N_{U_0}$  and similar) conserve the kinetic energy contained in the perturbation and averaged over the gap, namely  $E_t = E_0 + E_1 = (U_0^2 + W_0^2) + \sum_k \frac{1}{2}(U_k^2 + V_k^2 + W_k^2)$ . In this expression, it should be noticed that the first term does not possess the same  $1/2$  factor as the other terms, owing to the fact that it is the square average of a constant while the others are square averages of trigonometric lines. A second important feature is that it respects the linear stability of the plane Couette flow since the base flow  $u_b$  can be shown to be linearly stable for all Reynolds numbers, as was already demonstrated in Manneville and Locher [24] for the version truncated beyond  $k = 1$ .

Below, we present evidence gained by numerical simulations that the model reproduces transitional pCF reasonably well at a qualitative level and is worth studying further analytically.

### 3 Simulation results

Early numerical simulations were performed under conditions that correspond to experiments with a turbulent state prepared at high  $R$  and suddenly quenched at a lower  $R$  (Manneville [22]). These results were obtained with rather limited computing power in domains with periodic boundary conditions placed at short distances. An interesting feature is that, when the size of the computational domain is of the order of the wavelengths chosen by Waleffe [39], i.e.,  $L_x, L_z = \mathcal{O}(1)$ , a bifurcation diagram similar to his own is obtained, with  $R_g \sim 180$ . This could have been expected since it can be shown that his model is recovered from our model upon expanding the in-plane dependence of the fields in Fourier series and treating the nonlinear terms within a first-harmonic approximation. An important difference is, however, observed: here, the permanent regime is chaotic rather than stationary, and the global stability threshold is well understood in terms of a conversion of *chaotic transients* into a *chaotic attractor*, with all the usual fractal basin properties extending the complicated behavior described by Dauchot and Vioujard [10], and analogous to that described by Eckhardt and Mersmann [13].

We do not illustrate this transition further in order to focus more on spatio-temporal features that develop when the size of the domain gets larger. Simulation results presented in (Manneville [22]) were obtained in wide, but not so wide, domains with  $L_x = 32$ ,  $L_z = 16$ . A global stability threshold  $R_g \simeq 45$  was detected with transients similar to those observed below threshold  $R_g$  and sustained turbulence above. It should be noted that this value is quite low when compared to that obtained in the chaotic limit previously considered, which means that confinement effects play an important role and that spatial disorder significantly lowers every threshold obtained within the low-dimensional dynamical systems approach. By contrast, results described below concern the opposite wide-system limit. So a much larger domain with  $L_x = 128$  and  $L_z = 64$  was considered and the initial turbulent regime was produced by two successive doublings of the size at  $R = 100$ , adding noise to break the symmetry introduced by the doubling process. Sufficient time was given to the system to equilibrate and reach the sustained large- $R$  turbulent regime. A pseudo-spectral Fourier code

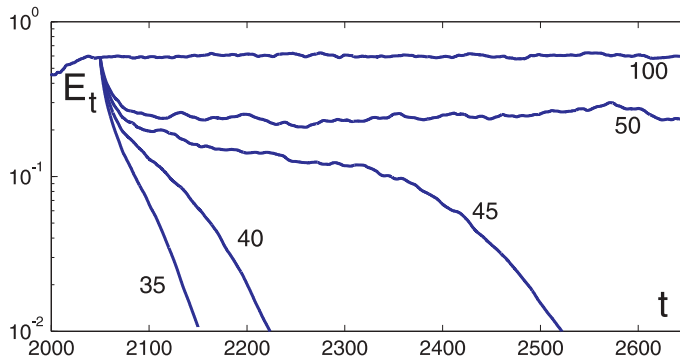


**Fig. 4.** Time series of the total perturbation energy in quench experiments

with alias removal by the 3/2 rule was developed and run on a NEC-SX5 computer (IDRIS at Orsay). We used  $1024 \times 512$  modes, equal space steps  $\delta x = \delta z = 0.125$  and a time step usually of order  $\delta t = 0.002$ . Temporal integration rested on a second-order Adams–Bashforth for the nonlinear terms, while the evolution due to all linear terms was evaluated exactly in Fourier space.

Quench experiments were first performed in order to make a link with previous experiments. Next the evolution of turbulent patches was studied. In the quench experiments, the system was launched from the initial turbulent state mentioned above at  $R = 100$  to ever smaller values of  $R$  that were maintained as long as necessary for the solution to reach the corresponding asymptotic regime. These experiments have first shown that, at given  $R$ , the average turbulent energy per unit surface was independent of the size in the long time limit so that the solutions to the model displayed an interesting extensivity property already for  $L_x \geq 32$  and  $L_z \geq 16$ . Second, as seen from Fig. 4, they confirmed the value of  $R_g \simeq 45$  obtained at the lowest size. This unrealistically low value, likely due to the choice of unphysical stress-free boundary conditions (as for convection), is of no concern in the qualitative perspective of our modeling approach. We now focus on numerical experiments dealing with the growth of turbulent spots and the coexistence of large turbulent and laminar domains.

The initial conditions were derived from a previously obtained homogeneous turbulent regime at  $R = 100$  by masking part of it in order to define the laminar region, i.e., by setting to zero the fields  $\psi_0$ ,  $\psi_1$ , and  $\phi_1$  outside domains of different shapes and connecting states smoothly at the boundary. Circular domains with small diameters served as initial conditions to study the nucleation of droplets. Bands, streamwise, spanwise, or oblique, were prepared to test the behavior of domain fronts between the laminar and turbulent states. Initial conditions were thus, by construction, acceptable velocity fields verifying the continuity condition automatically. Several values of the Reynolds number have been considered.

### 3.1 Growth of turbulent spots

Nucleation of the turbulent state from droplets of various sizes at different values of  $R$  has been studied. Here we consider the transition from a circular germ with very small radius ( $r \sim 2$ ). As understood from the left panel of Fig. 5, the spot decays for  $R = 50$  and  $R = 60$ . The perturbation is thus insufficient to trigger the homogeneous turbulent regime otherwise observed for these values of  $R$  in the quench experiments. By contrast, the right panel shows that the developed regime is obtained for  $R = 70$  after a transient in two steps. The initial growth stage resembles those for lower  $R$  but is now sufficiently large to make the solution tumble in the attraction basin of sustained turbulence. During the late stage this domain invades the whole system. Pictures of this evolution (local values of the total perturbation energy) at several successive times in the intermediate growth stage are displayed in Fig. 6.

Interestingly, as shown in Fig. 7 which displays the pattern obtained at early times from the same initial condition for several values of  $R$ , the very short term evolution of spots produces identical spatial structures independent of  $R$ , except for their amplitude. This behavior is expected from the conservative character of the nonlinear advection term as emphasized by Henningson and Reddy [16]. The only difference is the maximum energy reached that depends on  $R$ . In a phase space perspective this energy can be understood as an amplitude measuring distance to the origin (represented by the base state). This evolution stage thus corresponds mainly to transient non-normal linear amplification of the perturbation energy (Fig. 5, left). Nonlinear

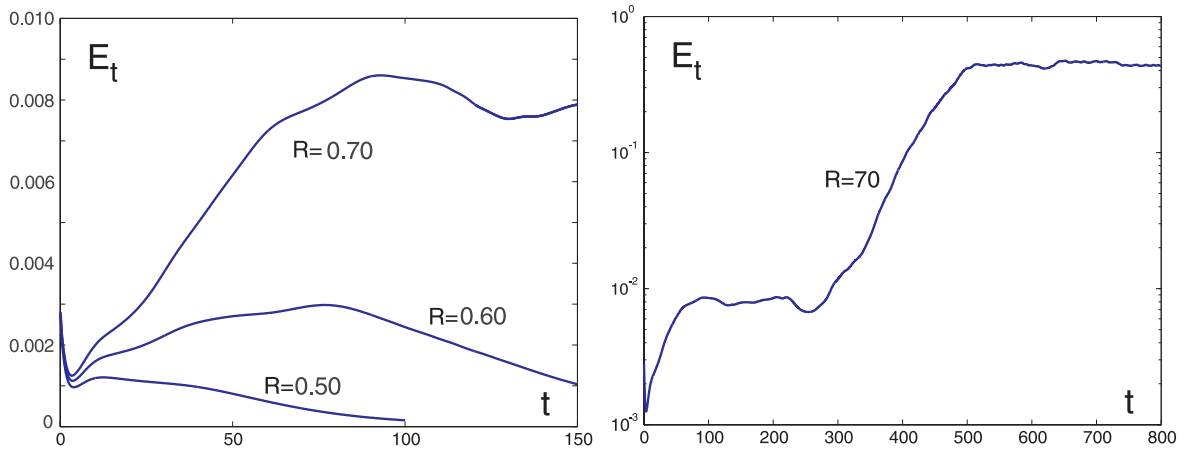


**Fig. 5.** Time series of the total perturbation energy  $E_t$ . Left: short term behavior for  $R = 70, 60,$  and  $50$  (lin-lin scales). Right: transition to the sustained turbulent regime for  $R = 70$  (lin-log scales)

effects then enter the game and, of course, patterns evolve differently at different  $R$  while keeping roughly the same shape, with well apparent streamwise structures (vortices and streaks). Comparing energy curves for  $R = 60$  and  $70$ , one clearly understands that the solution approaches some boundary in phase space but stays well inside the attraction basin of the base flow in the first case, while exploring a much more dangerous border region in the second case. The first plateau from  $t = 80$  to  $t = 250$  seen in Fig. 5 (right) for  $R = 70$  corresponds to a slow nonlinear evolution of the spot at roughly constant total perturbation energy, marked by an increase of its length and reorganization of the flow around it. Since our experiment is performed in a finite domain, periodic boundary conditions begin to be felt by the spot for  $t \sim 100$ . Later it takes the form of a streamwise turbulent band. The regular energy rise from  $t \sim 300$  to  $t \sim 500$  is associated to a slow regular widening of this streamwise turbulent band coexisting with laminar flow. The total perturbation energy then reaches a second plateau value after the shrinking of the laminar region has ended. The value of this energy is the same as that asymptotically obtained in quenched experiments at the corresponding Reynolds number.

### 3.2 Turbulent bands and fronts

The second experiment presented here focus more on the invasion stage observed during the late evolution of the spot studied above and more generally on the problem of front propagation separating turbulent from laminar domains.

Streamwise, oblique, and spanwise bands have been generated as initial conditions by following the procedure previously sketched. Whereas streamwise and spanwise bands can be prepared with any width, oblique bands could be produced with special angles in order to fit periodic boundary conditions. The relative width of laminar and turbulent bands that were obtained was not sufficient to lead to clear results about coexistence as a function of the angle, so that we shall consider only spanwise bands that have the most favorable width ratio. This limitation has now been raised by writing the system in a reference frame that makes an arbitrary angle with the direction of the base flow, a trick used by D. Barkley (private communication). The corresponding program is now currently developed by M. Lagha at LadHyX.

Snapshots of an evolving spanwise turbulent band is displayed in Fig. 8 for  $R = 70$ . The width of the turbulent domain grows and the final state is the expected homogeneous turbulent state. For  $R = 50$  (not shown) the band still seems to widen but turbulence finally decays in much the same way as it does in the quench experiment. In order to better visualize the profile of the solution and to point out the existence of a front (if any), we have performed an averaging of the local total perturbation energy over the width. The result of this crude, naive, but economic approach is presented in Fig. 9 as series of streamwise energy profiles taken every  $\Delta t = 5$  from  $t = 5$  to  $t = 40$ . Though the spatial development of the turbulent region is similar in both cases, the maximum of the total turbulent perturbation energy is observed to decay when  $R = 50$  indicating a collapse of turbulence, while expansion is observed when  $R = 70$ . The interesting result obtained is that the front moves definitely faster for  $R = 70$  than for  $R = 50$ , while in the latter case expansion of the turbulent

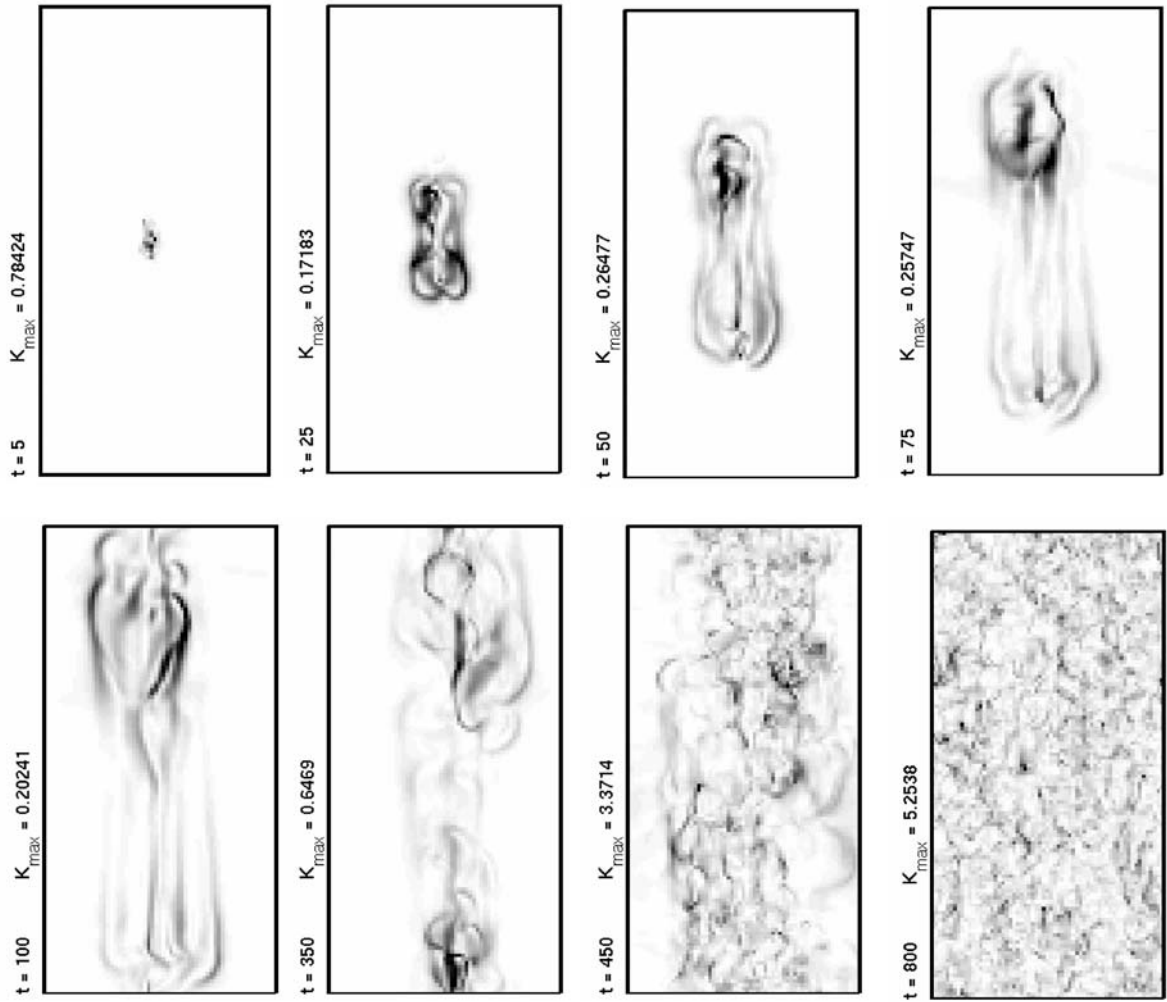


**Fig. 6.** Spatial distribution of the perturbation energy averaged over the gap in the solution nucleating from the small germ for  $R = 70$ . Gray levels from zero to the maximum value indicated in the left margin of each picture, together with the corresponding times. The streamwise (spanwise) coordinate is along the vertical (horizontal)

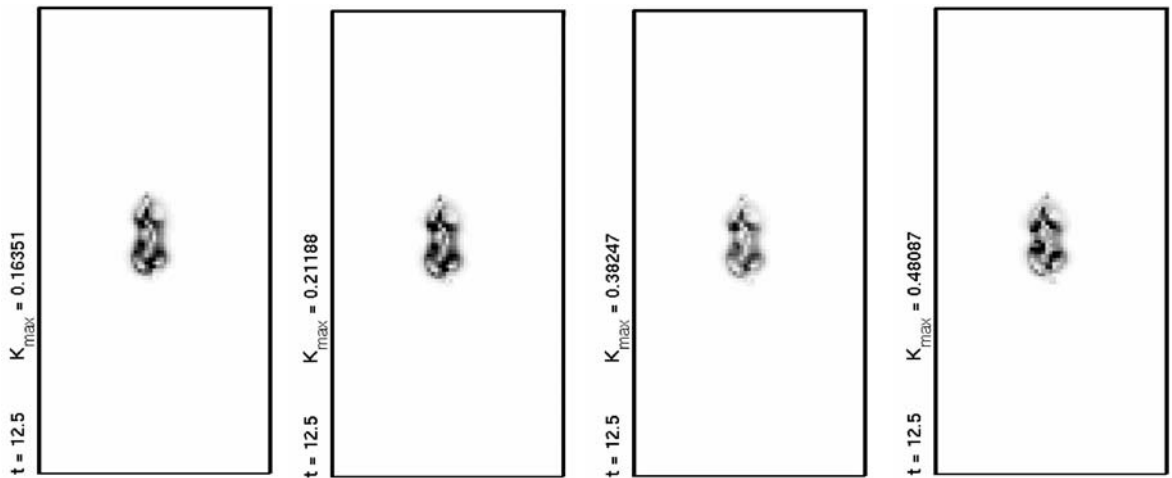


**Fig. 7.** Early spatial structure of spots evolving from the same initial condition for  $R = 50, 60, 70,$  and  $100$ . (Same graphical conventions as in Fig. 6)

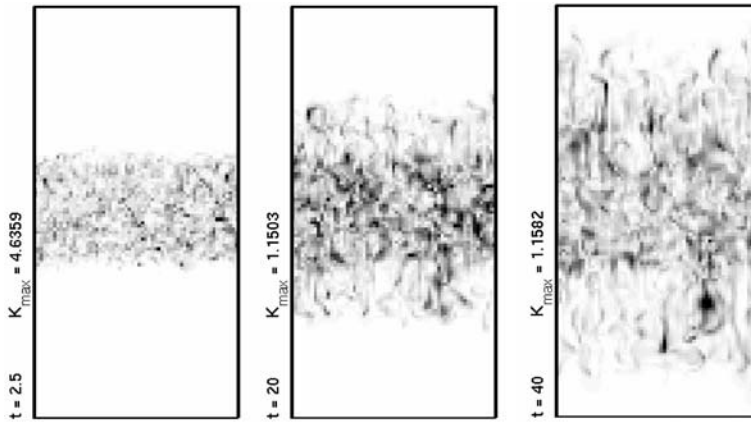


**Fig. 8.** Widening of the spanwise turbulent band for  $R = 70$ . (Same graphical conventions as in Fig. 6)

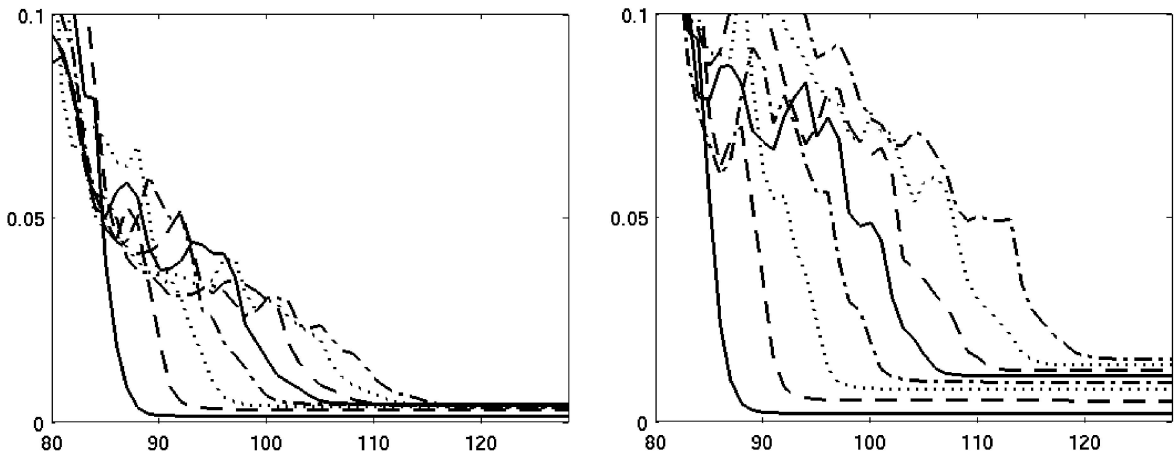


**Fig. 9.** Profile of the total turbulent perturbation energy averaged over the width of the system as a function of the streamwise coordinate. The initial condition is a spanwise turbulent band. Snapshots are taken every  $\Delta t = 5$  from  $t = 5$  (extreme left curve) to  $t = 40$  (extreme right curve). Left:  $R = 50$ , the turbulent region expands slowly but collapses. Right:  $R = 70$ , a well-defined advancing front is observed

region has to cope with its own breakdown, since close to  $R_g \simeq 45$  turbulence is long-lived only as long as it has a relatively uniform intensity, as it is the case in quenched experiments.

#### 4 Perspectives

Beyond the qualitative restitution of the globally subcritical behavior already reported before, it should be remarked first that our model mimics the growth of turbulent spots and stripes equally well. Not all our simulation results have been presented here. For the sake of conciseness we have dropped the account of less spectacular experiments with, e.g., wide germs, streamwise or oblique bands. On the other hand, more simulations are required to study close approaches to the boundary of the base-state attraction basin using the same initial condition as in the reported experiment but with different values of  $R$ , or the front velocity in the turbulent stripe experiment, or else other effects linked to the initial shape/intensity of the perturbation, in order to better situate this boundary. Even larger domains should also be considered in order to appreciate how tumbling to the invasion stage is dependent on the system's size.

Also, since it experimentally appears that oblique stripes are selected by the flow in the post-transitional regime where transition to featureless turbulence takes place, and since we have no real clue to this selection, i.e., problem (2), it would be interesting to check whether this property is already present in our model that is

more explicitly dedicated to the transitional regime, i.e., problem (1). Simulations of the modified program dealing with the oblique flow configuration are therefore planned for the near future.

Though efforts can certainly be made to improve the monitoring of the front position, interesting results have already been obtained, in particular that turbulence grows through advancing fronts but decays by local collapse rather than by receding fronts. This raises questions about one facet of the conjecture made by Pomeau [28] relative to the concrete applicability of the spatio-temporal intermittency scenario to the pCf case. In this respect, we must notice that front speeds should be studied from the coexistence of laminar and turbulent half-spaces, which makes our experiments still too sensitive to periodic boundary and finite size effects. In this limit, the competition between front motion and local collapse (at  $R = 50$  in the model) would in principle not happen and the turbulent domain would advance or recede rather by a slow erosion/contamination-like process. In laboratory experiments, similar limitations linked to size effects were observed except in the latest large aspect-ratio experiments by Prigent [29].

Interesting things happen in the model at unrealistically low values of  $R$  ( $R_g \sim 45$  in the model whereas  $R_g = 325$  in the laboratory experiments). This feature is not drastically changed by adding more fields to describe the cross stream dependence though an embryo of cascading transfer from modes 0 and 1 towards 2 (for which dissipation is more intense) begins to be seen, with a systematic ordering of energies contained in the different components of the flow,  $E_2 < E_1 < E_0$  (M. Lagha, private communication). The five-field model thus appears to be less pathological than the three-field model used here but this also suggests that the stress-free assumption plays the dominant role in the lowering of thresholds. This is already the case for convection where viscous dissipation is also underestimated but here the effect is more important probably because in convection a clear destabilizing mechanism is present already at the linear stage and the competition with dissipation has clear rules. This difficulty could be raised by turning to realistic no-slip boundary conditions and developing the Galerkin method on a different functional basis, e.g., polynomials that form a set appropriate to this case as already chosen for Rayleigh–Bénard convection in similar circumstances leading to (linear) results in excellent agreement with exact ones (Manneville [21], (b) Appendix A) but here the problem is fully nonlinear and truncation at lowest order might prove insufficient.

Finally, several of the different problems mentioned in Sect. 2, e.g., especially that of spots in plane Poiseuille flow or boundary layers and, above all, in transitional counter-rotating cCf are worth considering along the lines developed for pCf. Modeling the latter case focusing on the role of the average rotation rate is an appealing extension currently in progress.

*Acknowledgment.* Some of the results described here were presented at the 2003 Taylor–Couette Meeting in Barcelona (July 2003). Thanks are first due to the organizers for their kind invitation to give a talk at this interesting meeting. Computer time provided by IDRIS under project CP6/1462 is deeply acknowledged. Olivier Dauchot and his collaborators at GIT-SPEC Saclay, Bruno Eckhardt and his group in Marburg (German–French EGIDE exchange program PROCOPE under contract #04543RB), Carlo Cossu, Laurette Tuckerman and Dwight Barkley are all thanked for interesting discussions related to this study. Work is currently developed in collaboration with Maher Lagha, who obtained the results mentioned about the five-field model.

## References

1. Andereck, C.D., Liu, S.S., Swinney, H.L.: *J. Fluid Mech.* **164**, 155–183 (1986)
2. Bottin, S., Dauchot, O., Daviaud, F., Manneville, P.: *Phys. Fluids* **10**, 2597–2607 (1998)
3. Bottin, S., Daviaud, F., Manneville, P., Dauchot, O.: *Europhys. Lett.* **43**, 171–176 (1998)
4. Bottin, S., Chaté, H.: *Eur. Phys. J. B* **6**, 143–155 (1998)
5. Carlson, D.R., Widnall, S.E., Peeters, M.F.: *J. Fluid Mech.* **121**, 487–505 (1982)
6. Chapman, S.J.: *J. Fluid Mech.* **451**, 35–97 (2002)
7. Clever, R.M., Busse, F.H.: *J. Fluid Mech.* **234**, 511–527 (1992)
8. Coles, D.: *J. Fluid Mech.* **21**, 385–425 (1965)
9. Cros, A., Le Gal, P.: *Phys. Fluids* **14**, 3755–3765 (2002) [see their Fig. 13, the disagreement mentioned in the corresponding text disappears as soon as comparison is made not with  $R$  but with  $\bar{R} = 4R$  which is the physically relevant Reynolds number]
10. Dauchot, O., Vioujard, N.: *Eur. Phys. J. B* **14**, 377–381 (2000)
11. Drazin, P.G.: *Introduction to Hydrodynamic Stability*. CUP, Cambridge (2002)
12. Drazin, P.G., Reid, W.H.: *Hydrodynamic stability*. CUP, Cambridge (1981)
13. Eckhardt, B., Mersmann, A.: *Phys. Rev. E* **60**, 509–517 (1999)

14. Faisst, H., Eckhardt, B.: Phys. Rev. E **61**, 7227–7230 (2000)
15. Hamilton, J.M., Kim, J., Waleffe, F.: J. Fluid Mech. **287**, 317–348 (1995)
16. Henningson, D.S., Reddy, S.C.: Phys. Fluids **6**, 1396–1398 (1994)
17. Herbert, T.: Phys. Fluids **26**, 871–874 (1983)
18. Huerre, P., Rossi, M.: Hydrodynamic instabilities in open flows. Chapter 2 of *Hydrodynamics and Nonlinear Instabilities*, Cl. Godrèche and P. Manneville (eds.), CUP, Cambridge (1998)
19. Lorenz, E.N.: J. Atmos. Sc. **20**, 130–141 (1963)
20. Lundbladh, A., Johansson, A.V.: J. Fluid Mech. **229**, 499–516 (1991)
21. Manneville, P.: (a) J. Physique **44**, 759–765 (1983); (b) in *Cellular Structures in Instabilities*, Springer Lecture Notes in Physics **210**, 137–155 (1984)
22. Manneville, P.: Modeling transitional plane Couette flow. In: *Advances in Turbulence VIII*, C. Dopazo (ed.), CIMNE, Barcelona (2000). Proceedings of the ETC8 conference, pp. 75–78
23. Manneville, P., Dauchot, O.: Patterning and transition to turbulence in subcritical systems: the case of plane Couette flow. In: D. Reguera, L.L. Bonilla and J.M. Rubi (eds.), *Coherent Structures in Classical Systems*, Springer Verlag, Berlin (2001) pp. 58–79
24. Manneville, P., Locher, F.: C. R. Acad. Sc. IIB – Mécanique **328**, 159–164 (2000)
25. Manneville, P., Prigent, A., Dauchot, O.: Bull. Am. Phys. Soc. **46**, 35 (2001) [APS DFD01 San Diego 18–20 Novembre 2001]
26. Nagata, M.: J. Fluid Mech. **217**, 519–527 (1990)
27. Orszag, S.A.: J. Fluid Mech. **50** 689–703 (1971)
28. Pomeau, Y.: Physica D **23**, 3–11 (1986)
29. Prigent, A.: *La Spirale Turbulente: Motif de Grande Longueur d'Onde dans les Écoulements Cisailés Turbulents*, PhD Dissertation, Orsay/Paris-Sud University (2001)
30. Prigent, A., Grégoire, G., Chaté, H., Dauchot, O., van Saarloos, W.: Phys. Rev. Lett. **89**, 014501 (2002)
31. Prigent, A., Grégoire, G., Chaté, H., Dauchot, O.: Physica D **174**, 100–113 (2003)
32. Reddy, S.C., Schmid, P.J., Baggett, J.S., Henningson, D.S.: J. Fluid Mech. **365**, 269–303 (1998)
33. Romanov, V.A.: Funkt. Anal. Ego Prilo. **7**, 62–73 (1973)
34. Schmid, P.J., Henningson, D.S.: *Stability and Transition in Shear Flows*. Springer, Berlin (2001)
35. Schmiegel, A., Eckhardt, B.: Phys. Rev. Lett. **79**, 5250–5253 (1997)
36. Schumacher, J., Eckhardt, B.: Europhys. Lett. **52**, 627–632 (2000); Phys. Rev. E **63**, 046307-1–9 (2001)
37. Swift, J., Hohenberg, P.C.: Phys. Rev. A **15**, 319–328 (1977)
38. Trefethen, L.N., Trefethen, A.E., Reddy, S.C., Driscoll, T.A.: Science **261**, 578–584 (1993)
39. Waleffe, F.: Phys. Fluids **7**, 3060–3066 (1995)
40. Waleffe, F.: Phys. Fluids **9**, 883–900 (1997)